Neoplasia • Vol. 9, No. 9, September 2007, pp 734–744

www.neoplasia.com

B-FABP–Expressing Radial Glial Cells: The Malignant Glioma Cell of Origin?[1,2,3]

Raja Mita, Jeffrey E. Coles, Darryl D. Glubrecht, Rohyun Sung, Xuejun Sun and Roseline Godbout

Department of Oncology, University of Alberta, Cross Cancer Institute, Edmonton, Alberta, Canada T6G 1Z2

Abstract

Brain fatty acid–binding protein (B-FABP) is normally expressed in radial glial cells, where it plays a role in the establishment of the radial glial fiber network required for neuronal migration. B-FABP is also expressed in astrocytoma tumors and in some malignant glioma cell lines. To address the role of B-FABP in malignant glioma, we have studied the growth properties of clonal populations of malignant glioma cells modified for B-FABP expression. Here, we demonstrate that expression of B-FABP in B-FABP–negative malignant glioma cells is accompanied by the appearance of radial glial–like properties, such as increased migration and extended bipolar cell processes, as well as reduced transformation. Conversely, B-FABP depletion in B-FABP–positive malignant glioma cells results in decreased migration, reduction in cell processes, and a more transformed phenotype. Moreover, expression of B-FABP in astrocytomas is associated with regions of tumor infiltration and recurrence. Rather than being a direct manifestation of the tumorigenic process, we propose that the ability of high-grade astrocytoma cells to migrate long distances from the primary tumor reflects properties associated with their cell of origin. Thus, targeting B-FABP–expressing cells may make a significant impact on the treatment of these tumors.
Neoplasia (2007) **9,** 734–744

Keywords: Astrocytoma, radial glia, brain fatty acid–binding protein, migration, infiltration.

Introduction

Astrocytomas, classified as grades I to IV by the World Health Organization, are the most common central nervous system malignancies in humans. Grade III and grade IV astrocytomas, collectively referred to as high-grade malignant gliomas, are very aggressive, with patients diagnosed with these tumors having median survivals of 1.6 years and 5 months, respectively [1]. Although they have a higher survival rate, grade II astrocytomas frequently recur as high-grade astrocytomas, making the treatment of these tumors particularly challenging.

In spite of aggressive treatment often involving a combination of surgical resection, radiation therapy, and chemotherapy, patients with high-grade astrocytomas usually present with secondary brain tumors at sites that can be distal from the primary tumor mass. Yet extracranial spread of the disease is rare for high-grade astrocytomas, occurring in only 0.4% to 2.3% of patients [2,3]. The aggressive nature of high-grade astrocytomas may, therefore, reflect inherently migratory/infiltrative properties of the tumor cell of origin rather than acquired invasive properties. Astrocytomas are traditionally believed to arise from astrocytes because they express glial fibrillary acidic protein (GFAP), an astrocyte-specific marker. More recently, it has been suggested that these tumors may arise from pre-astrocytic transitional cells or multipotent neural stem cells [4].

We have previously reported that a subset of malignant glioma cell lines established from high-grade astrocytomas expresses brain fatty acid–binding protein (B-FABP; aka FABP7 or BLBP) [5]. During brain development, B-FABP is expressed in radial glial cells, where it plays a role in the establishment and maintenance of the radial glial fiber system that guides immature migrating neurons to their final destination [6,7]. The addition of anti–B-FABP antibodies to primary cultures of cerebellar cells blocks glial cell differentiation by preventing the extension of radial glial processes [6]. Radial glial cells give rise to GFAP-expressing astrocytes once neuronal migration is completed [8]. Radial glial cells also display properties of precursor cells, generating both neurons and glial cells *in vitro*, and have been proposed to function as neural progenitor or neural stem cells [9].

The FABP family consists of structurally related proteins that have cell-, tissue-, and development-specific patterns of expression. Roles for these proteins include the uptake and intracellular trafficking of fatty acids, bile acids, and retinoids, as well as roles in cell signaling, gene transcription, cell growth, and differentiation [10]. Fatty acids serve as precursors for signaling molecules, metabolic substrates, and membrane

Abbreviations: B-FABP, brain fatty acid–binding protein; GFAP, glial fibrillary acidic protein; DHA, docosahexanoic acid; PPAR, peroxisome proliferator–activated receptor

Address all correspondence to: Roseline Godbout, Cross Cancer Institute, 11560 University Avenue, Edmonton, Alberta, Canada T6G 1Z2. E-mail: rgodbout@ualberta.ca

[1]This article refers to supplementary material, which is designated by "W" (i.e., Figure W1) and is available online at www.bcdecker.com.

[2]This work was supported by the National Cancer Institute of Canada with funds from the Canadian Cancer Society and by a Research Initiative Program grant from the Alberta Cancer Board.

[3]This paper is dedicated to the memory of Dr. John Rowe.

Received 26 May 2007; Revised 4 July 2007; Accepted 6 July 2007.

DOI 10.1593/neo.07439

phospholipid constituents, and are mediators of gene expression [10]. Reports suggest a link between FABP levels and either increasing or decreasing malignancy. For example, liver and intestinal FABP levels decrease with the progression of liver and colon cancers, respectively [11,12]. Adipocyte FABP levels are higher in low-grade bladder carcinoma than in high-grade tumors [13], whereas epidermal FABP is expressed at higher levels in prostate cancer compared to prostatic hyperplasia [14]. Directly relevant to our study, a recent gene profiling analysis of grade IV astrocytoma revealed an inverse correlation between the expression of nuclear B-FABP and survival in patients younger than the median age [15].

Here, we address the role of B-FABP in the growth and migration properties of malignant glioma cells. We report that stable introduction of a B-FABP expression construct into a B-FABP–negative malignant glioma cell line reduces its anchorage independence and enhances its migratory properties. Conversely, reduction of B-FABP in B-FABP–positive cells reduces its migratory properties. Analysis of B-FABP distribution in astrocytoma tumors indicates elevated levels of B-FABP in infiltrating regions of the tumors. Our results suggest an important role for B-FABP in controlling the migration of malignant glioma cells. Based on our *in vitro* and *in vivo* studies, we propose that B-FABP expression in astrocytoma tumors drives the infiltration of malignant cells into adjacent brain tissues.

Materials and Methods

Stable Transfections

Cells were transfected by calcium phosphate–mediated DNA transfection. The B-FABP expression construct was prepared by inserting a 467-bp human B-FABP cDNA fragment containing the entire open reading frame into the pREP4 vector, which carries the gene for hygromycin resistance. The pSUPER RNAi system (Oligoengine, Seattle, WA) was used to reduce levels of B-FABP in U251 cells. A 64-bp inverted repeat-containing sense/antisense 19-nt gene-specific sequence (CCAACGGTAATTATCAGTC; corresponding to B-FABP nt 114–132) was introduced into the pSUPER vector at the *Bgl*II/*Hin*dIII site. For stable transfectants, pSUPER vectors were cotransfected with a pREP4 empty vector. U87- and U251-transfected cells were selected in 400 μg/ml hygromycin, and individual colonies were picked using cloning rings.

Western Blot Analysis

Whole-cell lysates were electrophoresed in 13.5% SDS polyacrylamide gels, followed by electroblotting onto nitrocellulose. Blots were immunostained with rabbit anti–B-FABP antibody prepared by immunizing rabbits with recombinant glutathione *S*-transferase (GST)–tagged human B-FABP (1:1000 dilution) [5] or goat anti-actin antibody (1:5000 dilution; Santa Cruz Biotechnology, Santa Cruz, CA). Primary antibodies were detected with horseradish peroxidase–conjugated secondary antibodies (Jackson ImmunoResearch Laboratories, West Grove, PA) using the ECL detection system (GE Healthcare, Baie d'Urfe, Canada).

Cell Motility, Migration, and Invasion

Nondirectional cell motility was measured by 2D time-lapse video microscopy. Cells were plated in triplicate (75,000 cells/35-mm tissue culture dish) and cultured for 24 hours. Metamorph imaging software was used to capture a single differential interference contrast (DIC) image every 30 seconds for 2 hours (241 images in total), with each image containing 30 to 40 cells. A video was then constructed, and the migration of single cells was tracked using the Metamorph tracking function. Directional cell migration was measured by plating 25,000 cells in DMEM in the upper chamber of Transwell culture dishes (BD Falcon Labware, Bedford, MA). Cells were allowed to migrate through an 8-μm polyethylene terephthalate (PET) membrane toward a chemoattractant (DMEM + 10% fetal calf serum in a bottom chamber) for 6 hours. Cells were then fixed in 70% methanol and stained with 1% crystal violet. Cells were photographed and counted using Metamorph cell-counting software. Cell invasion was measured using BD Biocoat Matrigel invasion chambers (BD Biosciences, San Jose, CA) following the manufacturer's directions. Top chambers were plated with either 10,000 cells (for U87 transfectants) or 25,000 cells (for U251 transfectants) in DMEM and incubated for 22 hours. Cells were fixed, stained, and counted as described for the Transwell migration assay.

Immunofluorescence and Immunohistochemical Analysis

For immunofluorescence analysis, cells growing on coverslips were fixed in 1% paraformaldehyde in phosphate-buffered saline for 10 minutes and permeabilized in 0.5% Triton X-100 for 5 minutes. The cells were colabeled with affinity-purified rabbit anti–B-FABP (1:200 dilution) followed by Alexa-488 goat anti-rabbit (1:200 dilution) (Cedarlane Laboratories, Burlington, Canada) and with Alexa-546 phalloidin (1:200 dilution) (Molecular Probes; Invitrogen, Carlsbad, CA). Affinity purification of rabbit anti–B-FABP antibody [5] was performed using Hi-Trap NHS-activated Sepharose columns (GE Healthcare) linked to GST 4B–purified GST-B-FABP. Images were collected on a Zeiss (Oberkochen, Germany) LSM 510 confocal microscope with a 40×/1.3 oil immersion lens.

For immunohistochemical analysis, grade II and grade IV astrocytomas embedded in paraffin were obtained from the Department of Pathology and Laboratory Medicine, University of Alberta (Edmonton, Alberta, Canada), or from the Brain Tumor Tissue Bank, London Health Sciences Center, London (Canada). Tissues were deparaffinized in xylene, rehydrated, microwaved for 20 minutes in citrate/Tween-20 epitope retrieval buffer (pH 6), and incubated in affinity-purified anti–B-FABP antibody (1:800 dilution) overnight at 4°C. Slides were washed and incubated for 1 hour in DakoCytomation EnvisionPlus anti-rabbit secondary antibody (DakoCytomation, Glostrup, Denmark). Immunoreactivity was detected using DakoCytomation Liquid DAB$^+$ Substrate Chromagen System (DakoCytomation). The slides were counterstained with hematoxylin. A low-magnification picture of the entire

tissue section shown in Figure 6 was generated by taking 28 low-magnification pictures of the tissue and merging them using Adobe Photoshop (Adobe Systems Incorporated, San Jose, CA).

Results

Stable B-FABP Transfection of U87 Cells

To address the role of B-FABP in malignant glioma cells, we stably transfected the B-FABP–negative U87 malignant glioma cell line with a pREP4/B-FABP expression construct. U87 cells transfected with an empty vector served as the control for these experiments. Control and B-FABP–transfected cells were selected in hygromycin, and individual colonies were picked using cloning rings.

B-FABP levels in four stable B-FABP transfectants (U87-B1, U87-B2, U87-B3, and U87-B4) were examined by Western blot analysis. As shown in Figure 1*A*, all four B-FABP transfectants expressed B-FABP, with the highest levels observed in U87-B4. B-FABP levels in U87-B4 were similar to endogenous B-FABP levels found in B-FABP–expressing U251 cells, with approximately three-fold lower levels observed in U87-B1, U87-B2, and U87-B3. As expected, B-FABP was not detected in the three pREP4 control transfectants U87-(pREP4)R1, U87-R2, and U87-R3.

Depletion of B-FABP in U251 Cells

U251 cells express endogenous B-FABP. We used RNA interference to reduce B-FABP levels in these cells. The pSUPER vector was used for these experiments because it allows long-term reduction in protein levels as a result of the persistent production of short hairpin RNA in stable transfectants. Nucleotides 114 to 132 of the B-FABP coding region served as our target sequence, with pSUPER empty vector serving as the control. To select stable transfectants, pSUPER constructs were cotransfected with pREP4 and cells were selected in hygromycin. These colonies were expanded and analyzed for B-FABP expression after at least 10 passages of a subconfluent culture in a 100-mm plate. A 70% to 90% reduction in B-FABP levels was observed in three U251 pSUPER/B-FABP transfectants, labeled U251-B1, U251-B2, and U251-B3 (Figure 1*B*). All three control transfectants [S(pSUPER)1, S2, and S3] showed significantly higher levels of B-FABP compared to pSUPER/B-FABP transfectants.

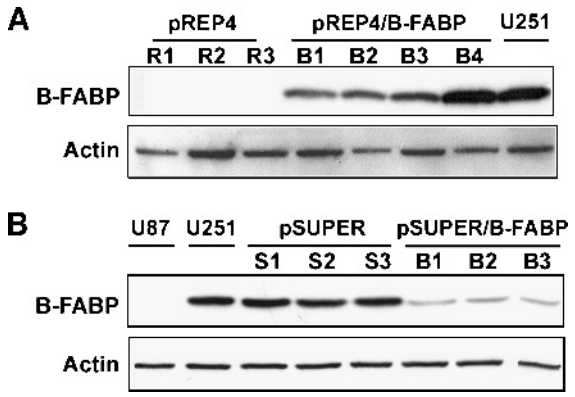

Figure 1. *Western blot analysis of B-FABP in U87- and U251-transfected cells. (A) Whole-cell extracts (50 μg/lane) were prepared from U87 cells stably transfected with empty pREP4 vector (R1, R2, and R3), U87 cells stably transfected with pREP4/B-FABP (B1, B2, B3, and B4), and U251. (B) Whole-cell extracts (50 μg/lane) were prepared from U251 stably transfected with empty pSUPER vector (S1, S2, and S3) and pSUPER/B-FABP (B1, B2, and B3). Extracts were electrophoresed on a 13.5% SDS polyacrylamide gel. Proteins were transferred to nitrocellulose membranes and sequentially immunostained with rabbit anti–B-FABP antibody and goat anti-actin antibody, followed by horseradish peroxidase–conjugated secondary antibodies.*

Morphologic Changes in U87 and U251 Transfectants

We used phase-contrast microscopy to study the morphology of B-FABP–negative U87, control transfectants, and B-FABP–expressing transfectants. The U87 parent cell line and control transfectants generally had a stellate appearance with short processes (Figure 2*A*, *top panels*). In contrast, B-FABP–expressing U87 cells formed extended bipolar processes (indicated by *arrowheads*) often spanning considerable distances (as much as 250 μm) (Figure 2*A*, *bottom panels*). These elongated processes are similar in appearance to radial glial processes that can span the entire width of the cortical wall during brain development [16].

U251 cells generally form longer processes compared to U87 cells, with the processes often having a bipolar appearance. The morphology of all three U251 control transfectants was similar to that of the parent U251 cells (Figure 2*B*, *top panels*). Depletion of B-FABP in U251-B1, U251-B2, and U251-B3 resulted in loss of elongated processes and the formation of fan-like structures (indicated by *arrowheads*) usually associated with extensive membrane ruffling (Figure 2*B*, *bottom panels*). These fan-like structures were mainly observed when the cells were subconfluent. No difference in cell piling was observed for any of the transfectants at confluence.

B-FABP Expression and Cell Migration

B-FABP expression in malignant glioma cells results in the formation of elongated processes that may be associated with cell migration. We used two different approaches to study the effect of B-FABP on malignant glioma cell motility: 1) 2D time-lapse video microscopy, which measures random (or nondirected) movement; and 2) Transwell chambers, which are used to measure directed migration toward a chemoattractant (10% fetal calf serum).

Using 2D time-lapse video microscopy, we followed the total movement of ~ 100 cells per U87 clone over a period of 2 hours (30–40 cells were analyzed per experiment). All four U87 B-FABP transfectants had a higher motility rate than control transfectants, with B-FABP–expressing U87 clones traveling at 75 to 94 μm/hr compared to 48 to 58 μm/hr for controls (Figure 3*A*). Differences in motility were found to be statistically significant using unpaired *t*-test ($P < .001$). Similar results were obtained with Transwell chambers, with B-FABP–expressing transfectants being highly migratory compared to control transfectants. A range of 1997 to 2997 cells migrated through the porous filter toward the chemoattractant in the case of U87 B-FABP transfectants, in contrast to 273 to

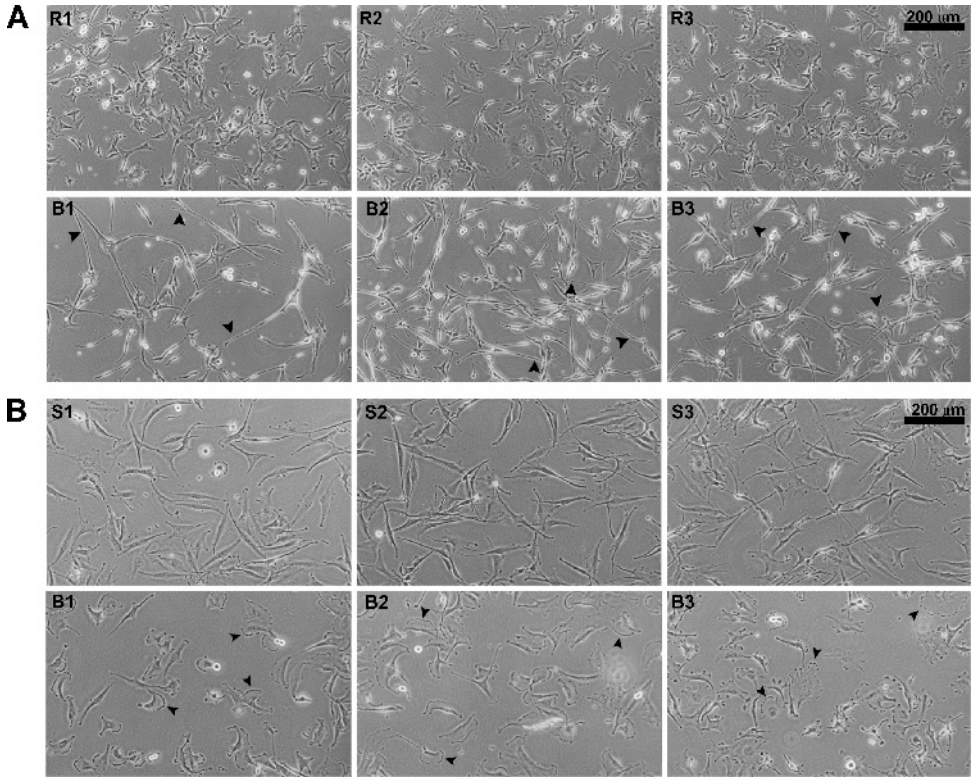

Figure 2. *Morphologic analysis of U87- and U251-transfected cells. (A) Phase-contrast microscopy was used to study the morphology of U87 cells stably transfected with either pREP4 (R1, R2, and R3) or the pREP4/B-FABP expression construct (B1, B2, and B3). Arrowheads point to elongated processes observed in U87 pREP4/B-FABP transfectants. (B) Phase-contrast analysis of U251 cells stably cotransfected with pSUPER (S1, S2, and S3) or pSUPER/B-FABP (B1, B2, and B3) and pREP4. Arrowheads point to the extensive membrane ruffling observed in U251 B-FABP knockdowns.*

816 cells in the case of U87 control transfectants (Figure 3*C*). U87 B-FABP4, with the highest levels of B-FABP, had the highest number of migrating cells. These differences in migration were highly significant ($P < .0001$).

Similar analyses carried out with B-FABP–depleted and control U251 transfectants support a role for B-FABP in cell motility. 2D time-lapse video microscopy revealed higher motility rates for U251 control transfectants, ranging from 60 to 63 μm/hr, compared to B-FABP–depleted U251 clones, which ranged from 43 to 52 μm/hr ($P < .001$) (Figure 3*B*). Results from Transwell chambers showed decreased migration as a function of B-FABP depletion, with 1726 to 1890 cells/well for U251 control transfectants compared to 617 to 950 cells/well for B-FABP–depleted U251 transfectants ($P < .0001$) (Figure 3*D*).

B-FABP Expression and Invasion

We used the *in vitro* Matrigel invasion assay to determine whether the increased migration rate associated with B-FABP expression in malignant glioma cells corresponded to an increase in invasive properties. The Matrigel matrix is a reconstituted basement membrane that is coated over a filter with 8 μm pore size. The basement membrane prevents noninvasive cells from migrating through the filter. This assay has been widely used to study the invasive properties of malignant glioma cells and has been shown to correlate well with the 3D spheroid invasion assay and the *in vivo* intracranial implantation assay [17].

U87- or U251-transfected cells were plated in the upper compartments of Matrigel chambers and incubated at 37°C for 22 hours. Cells that were able to pass through the Matrigel matrix during this time period were stained and counted. There was a trend toward increased cell invasion as a result of B-FABP expression in U87 ($P < .026$), with 77 to 136 cells/well in the control group compared to 114 to 236 cells/well in the B-FABP–expressing group (Figure 3*E*). An approximately two-fold reduction in the number of invading cells was observed in B-FABP–depleted U251 cells compared to controls ($P < .0001$) (Figure 3*F*).

B-FABP Expression, Cell Proliferation, and Anchorage Independence

The doubling times of B-FABP–transfected U87 and B-FABP–depleted U251 were measured at 24-hour intervals when cells were in the exponential growth phase. B-FABP expression in U87 cells resulted in a significant decrease in proliferation rate. Doubling times ranged from 28 to 32.5 hours in control transfectants and from 49 to 77 hours in B-FABP transfectants (Figure W1). In contrast, no significant changes in doubling times were observed in U251 control transfectants compared to B-FABP–depleted U251 transfectants.

B-FABP has been postulated to be associated with radial glial cell differentiation and process formation [6]. B-FABP expression in malignant gliomas, therefore, may not only

enhance migration properties but also be a hallmark of increased cell differentiation and decreased cell transformation. Anchorage-independent growth is an *in vitro* transformation assay that correlates well with tumor formation in nude mice [18]. U87 and U251 transfectants were plated in soft agar, and colonies > 50 cells were counted after 4 weeks in culture. B-FABP expression in U87 cells resulted in a significant decrease in soft agar growth, with an average of 12 to 118 colonies/plate for U87 B-FABP transfectants, compared to an average of 255 to 333 colonies/plate for control transfectants ($P < .0001$) (Figure W2). A difference, albeit of smaller magnitude, was also noted between U251 control and B-FABP–depleted transfectants, with an average of 290 to 387 colonies/plate observed in B-FABP–depleted

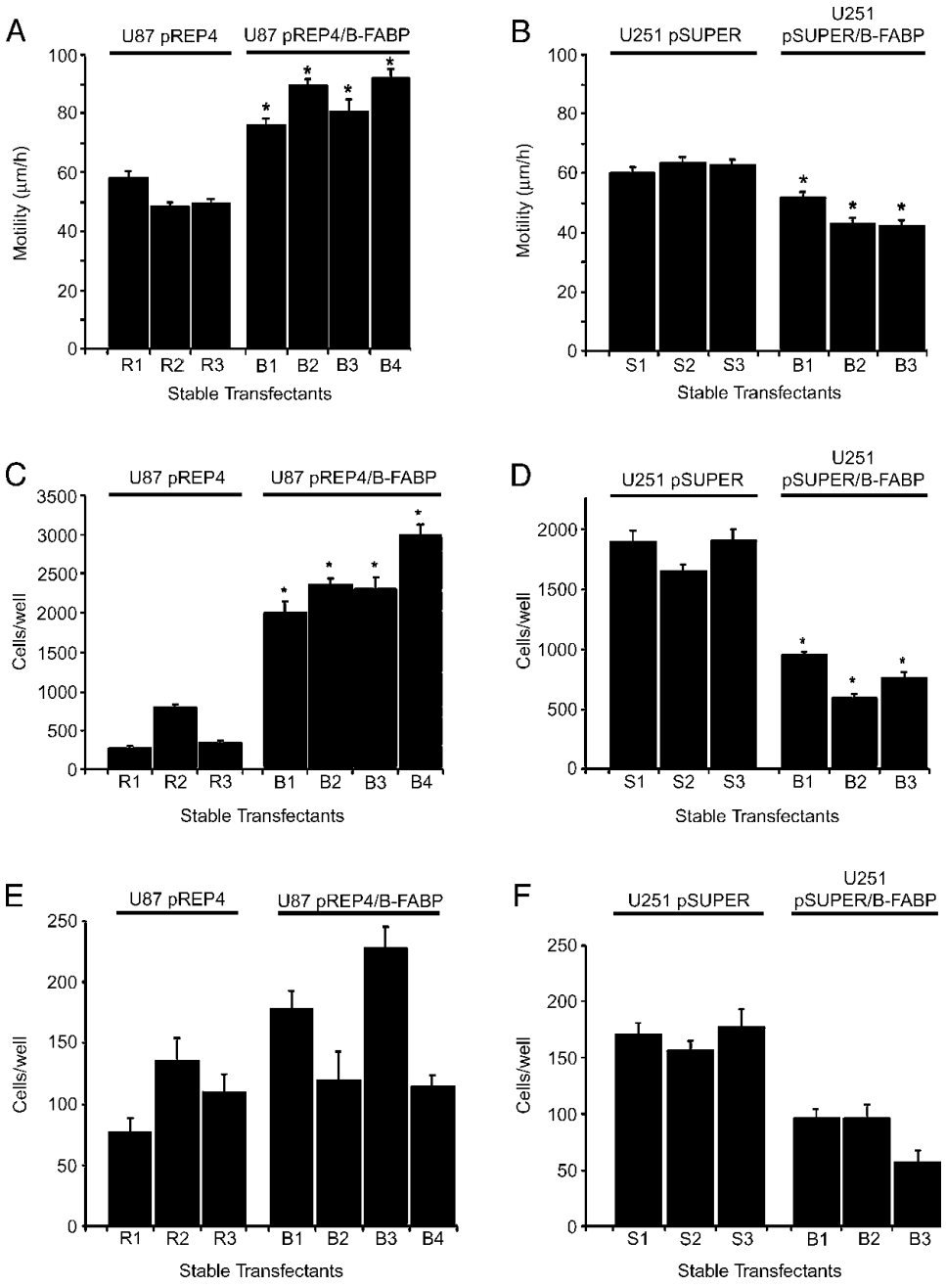

Figure 3. *Cell motility, migration, and invasion of U87- and U251-transfected cells. The nondirectional motility of U87 (A) and U251 (B) transfectants was measured using 2D time-lapse video microscopy. Cells were plated in triplicate on 35-mm tissue culture dishes and imaged with phase-contrast optics using a Zeiss Axiovert microscope with a 10× lens. The movement of 90 to 120 cells (30–40 cells/plate; three plates) was followed over a period of 2 hours, with pictures taken at 30-second intervals. Distances were measured using the Metamorph tracking function. Statistical significance was determined using unpaired t-test. Error bars represent the standard error of the mean (SEM). (C and D) The cell migration of U87 (C) and U251 (D) transfectants was measured using the Transwell assay (Falcon Labware). Twenty-five thousand cells were plated in triplicate and incubated for 6 hours, and the cells migrating through the porous membrane were fixed, stained, and counted using Metamorph imaging software. Statistical significance was determined using unpaired t-test. Error bars represent standard deviation. (E and F) Matrigel invasion of U87-transfected cells (E) and U251-transfected cells (F) using Matrigel invasion chambers. For U87 transfectants, 25,000 cells were plated, incubated for 22 hours, and stained. For U251 transfectants, 10,000 cells were plated, incubated for 22 hours, and stained. Error bars indicate SEM.*

transfectants compared to an average of 225 to 230 colonies/plate in control transfectants ($P < .008$).

Subcellular Localization of B-FABP in Malignant Glioma Cell Lines

Cell migration involves protrusion and adhesion in front of the cell, contraction of cell body, and detachment at the rear [19]. These processes require actin cytoskeleton remodeling involving actin polymerization/depolymerization and are regulated by small GTPases [20,21]. We used immunofluorescence microscopy to study the subcellular distribution of B-FABP in relation to filamentous actin. As shown in Figure 4*A*, B-FABP is enriched in the nuclei of U251 control transfectants and is concentrated at the leading edge of the cells (*arrow*). There is extensive staining of F-actin at the leading edge of U251 cells, and actin stress fibers are abundant in these cells (Figure 4*B*). Interestingly, there is a significant amount of colocalization between B-FABP and F-actin in U251 cells (Figure 4*C*), implying a possible association between B-FABP and F-actin. B-FABP–depleted U251 cells demonstrate a reduction in F-actin at the plasma membrane, as well as a reduced number of stress fibers (Figure 4, *D* and *E*). There is little colocalization of B-FABP and F-actin in these cells (Figure 4*F*). B-FABP–expressing U87 cells (U87 B-FABP3) have a staining pattern similar to that observed in U251 control transfectants (Figure 4, *G–I*).

Distribution of B-FABP in Astrocytoma Tumors

Immunohistochemical analysis of a grade II astrocytoma indicates B-FABP expression in gemistocytic astrocytes

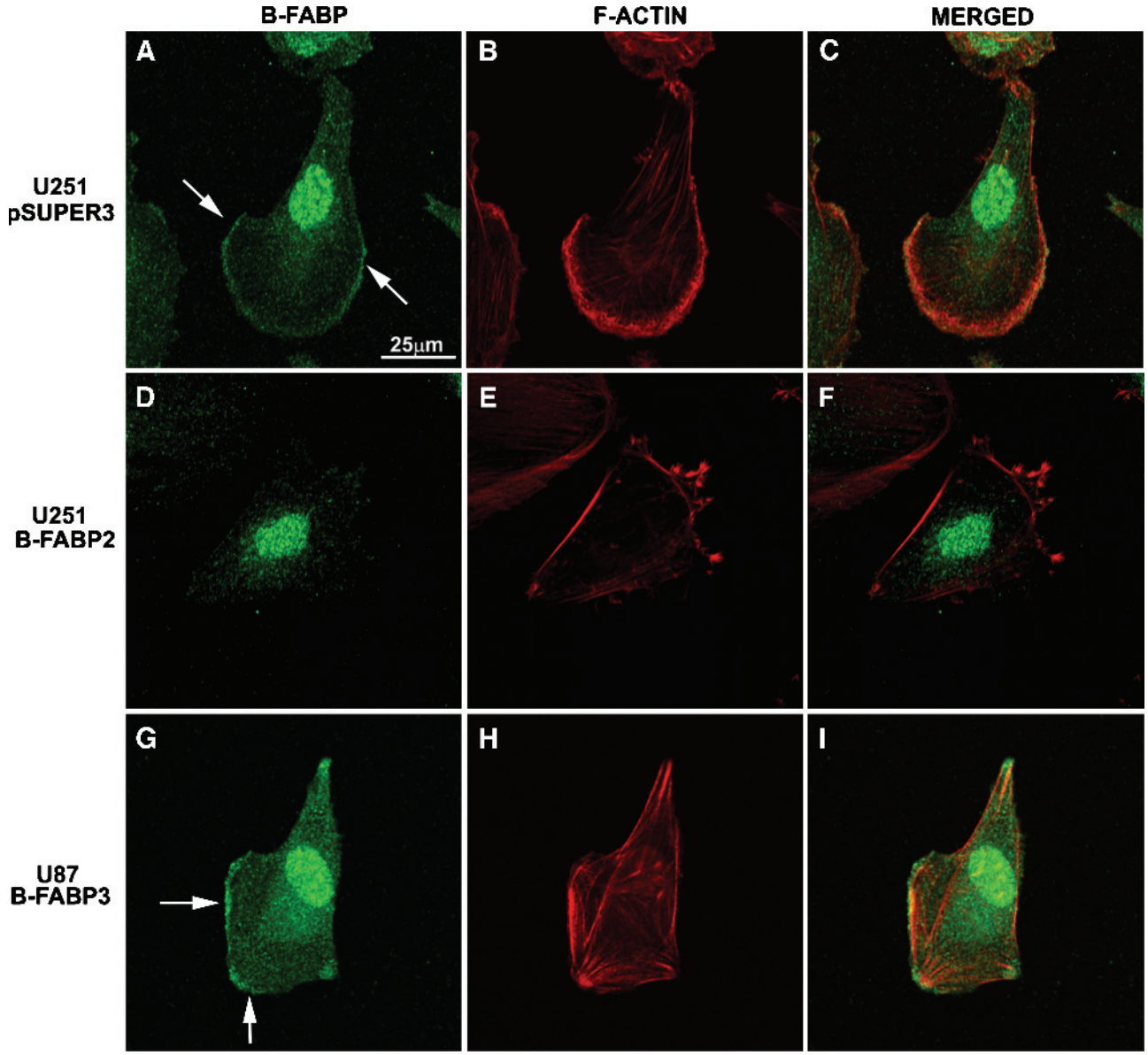

Figure 4. *Subcellular localization of B-FABP in U87 and U251 transfectants. The subcellular location of B-FABP in U251 pSUPER3 control (A–C), U251 pSUPER/B-FABP2 (D–F), and U87 B-FABP3 (G–I) was analyzed by immunofluorescence using (i) anti–B-FABP primary antibody followed by Alexa-488–conjugated secondary antibody (A, D, and G) and (ii) Alexa-546 phalloidin, which stains F-actin (B, E, and H). B-FABP and F-actin signals were merged in (C), (F), and (I).*

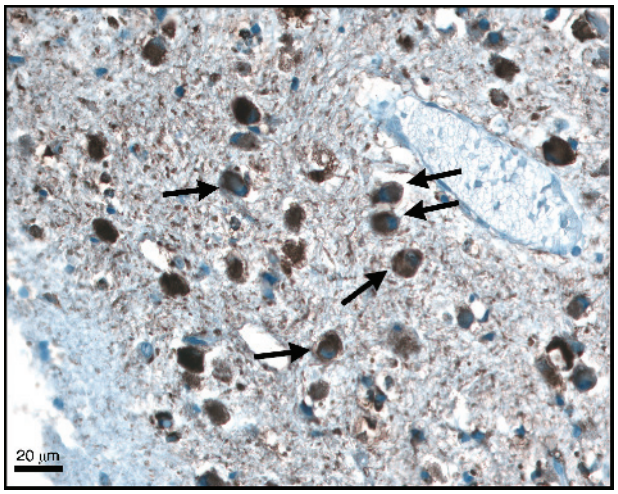

Figure 5. *Immunohistochemical analysis of B-FABP in grade II astrocytoma. The tissue section was immunostained with affinity-purified anti–B-FABP antibody and counterstained with hematoxylin. Arrows point to B-FABP–positive gemistocytic astrocytes.*

(Figure 5). Although gemistocytes have a low proliferative index, their presence in astrocytomas is considered a sign of poor prognosis, with gemistocyte-rich tumors rapidly progressing to high-grade astrocytomas [22,23]. Immunohistochemical analysis of grade IV astrocytomas revealed considerable variation in B-FABP expression, as previously reported [24,25]. As we were particularly interested in the role of B-FABP in migration and infiltration, we selected tumors for analysis that contained regions of high infiltration based on pathology reports. In Figure 6, we show a grade IV astrocytoma specimen (patient 670) that contains the following tissue grades: 1 = *no visible tumor cells*; 2 = *scant tumor cells*; 3 = *tumor center*; and 4 = *heavy tumor infiltration of the central nervous system parenchyma*. The *top panel* shows a low-magnification view of tissue immunostained with anti–B-FABP antibody and counterstained with hematoxylin. The cortical tissue on the left is characterized by low cellularity, with weak B-FABP staining that is mostly cytoplasmic (*panel 1*). B-FABP staining is stronger in *panel 2* but remains primarily cytoplasmic, although some B-FABP–positive nuclei are observed. The tumor center (*panel 3*) is characterized by high cellularity, with ~ 25% of nuclei staining positive for B-FABP. Regions of the tumor classified as heavy tumor infiltrates (*panel 4*) show high cellularity, numerous blood vessels, and abundant nuclear and cytoplasmic B-FABP staining, especially in cells located in the vicinity of blood vessels. The surrounding of blood vessels by B-FABP–positive cells was commonly observed in grade IV astrocytomas (e.g., patient 1022; Figure 7*A*). Accumulation of B-FABP–expressing cells in the subpial region of the brain was also observed in grade IV astrocytoma (e.g., patient 1032; Figure 7*B*).

Discussion

Despite recent advances in the treatment of high-grade astrocytomas, prognosis for these patients remains dismal. Current therapies are effective at destroying cells within or near the primary tumor mass; however, we still have no way of identifying and targeting malignant cells that have migrated away from the main tumor. As a result, patients with high-grade astrocytomas consistently relapse, presenting with secondary tumors that can be within 1 to 2 cm of—or much more distant from—the primary tumor site. We need to find ways of targeting malignant cells that infiltrate the brain if we are to make an impact on the treatment of these tumors.

We have previously shown that the radial glial marker B-FABP is expressed in astrocytoma tumors and malignant glioma cell lines [5]. In addition to serving as a scaffold for neuronal migration, radial glial cells can transform into GFAP-expressing astrocytes and can also function as neuronal cell progenitors [8,26]. Radial glial cells proliferate throughout neurogenesis [27] and demonstrate neural stem cell–like properties in embryonic and adult mice brains [28]. Two large-scale DNA microarray studies have shown an association between B-FABP expression and astrocytomas. In one study, B-FABP was identified as one of the top 100 genes expressed at significantly higher levels in primary grade IV astrocytomas compared to normal brain tissues [29]. In the second study, nuclear B-FABP expression was shown to correlate with a worse prognosis in astrocytoma grade IV patients below the median age [15]. A comparison of B-FABP levels in grade I *versus* grade II/III/IV astrocytomas and an analysis of cytoplasmic *versus* nuclear B-FABP levels in grade IV astrocytomas as a function of survival also support a link between nuclear B-FABP expression and invasion/infiltration [24,25].

Using two different assays for cell motility, one nondirectional (time-lapse video microscopy) and the other directional (Transwell chambers), we have observed striking differences in the migration of B-FABP–expressing *versus* B-FABP–negative/depleted clonal cell populations, with the former showing much higher motility. These results are consistent with a previous report demonstrating an increase in migration when SF767 malignant glioma cells (which express low levels of B-FABP) are transiently transfected with a B-FABP expression construct [15]. Although we also observe increases in cell invasion in B-FABP–expressing clones compared to B-FABP–negative/depleted clones, this could be due to increased cell motility. Thus, a major consequence of B-FABP expression in malignant glioma cells is enhancement of their motility.

Radial glial cells are traditionally believed to be static, with neuronal progeny migrating along radial glial fibers. However, recent evidence suggests that radial glial cells are much more than migratory guides, generating radial glial daughter cells that migrate away from parent cells, form extended processes, and become neurons [30]. Furthermore, the migration of radial glial cells by somal translocation has been documented in mouse, rat, and monkey brains [8,31,32]. In addition to longer processes, B-FABP expressing U87 cells have a distinctive migratory behavior resembling translocation (i.e., extension of the leading process followed by forward snapping of the cell body) as opposed to locomotion (i.e., movement of the entire cell) [33]. In contrast, the

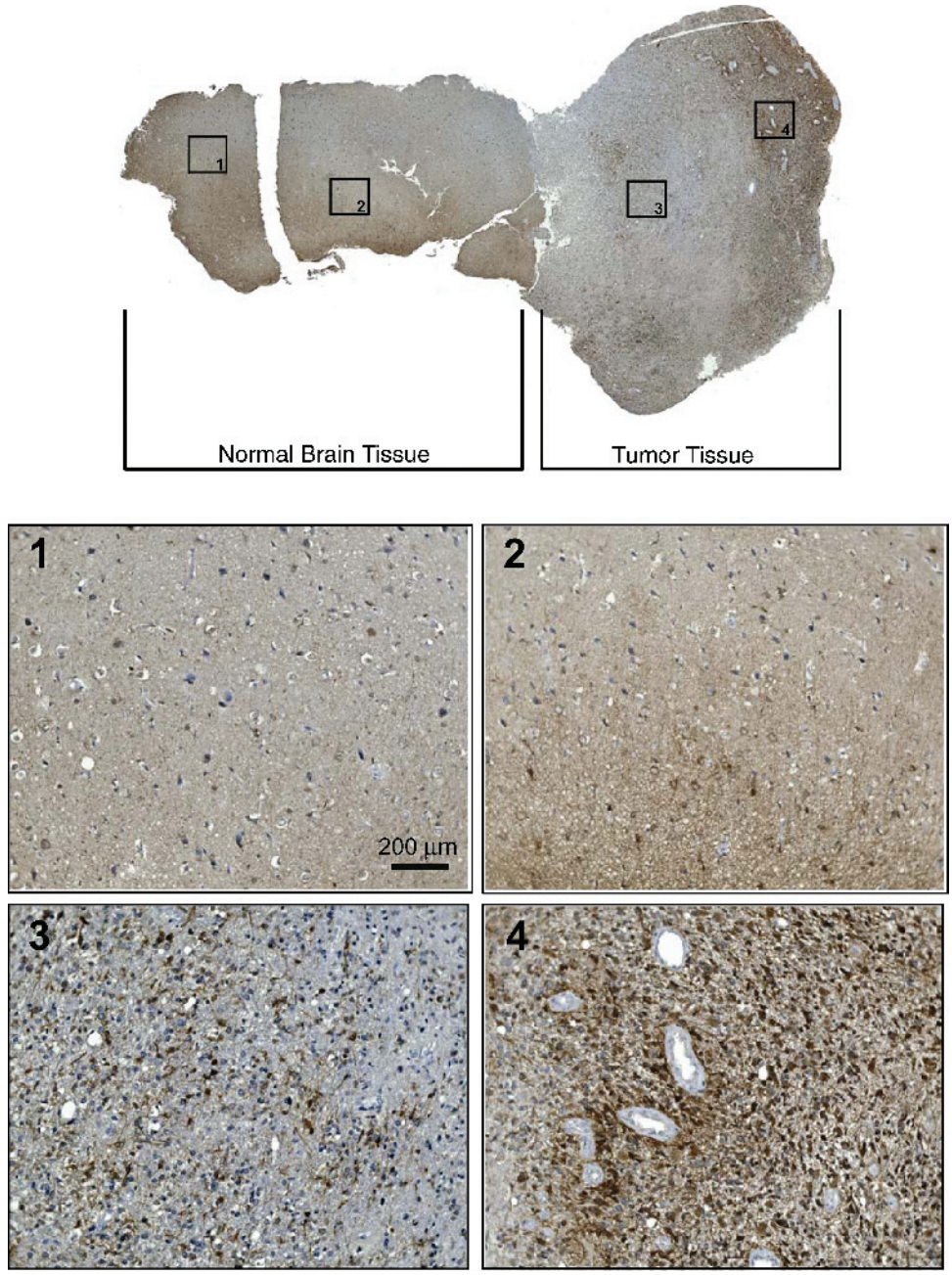

Figure 6. *Immunohistochemical analysis of B-FABP in grade IV astrocytoma (patient 670). The tissue section was immunostained with affinity-purified anti–B-FABP antibody and counterstained with hematoxylin. Top diagram: A low-magnification view of the entire section consisting of normal cortex and tumor tissue. Areas labeled 1 (*no visible tumor cells*), 2 (*scant tumor cells*), 3 (*tumor center*), and 4 (*heavy tumor infiltration of the central nervous system parenchyma*) are enlarged in the bottom panels.*

reduction of B-FABP levels in U251 results in fan-like membrane ruffling with almost no extended protrusions. Although membrane ruffling is associated with increased cell motility, it is the specific concentration of membrane ruffling at the ends of lamellipodia–filopodia extensions that has been linked to this process [34]. Fan-like structures, such as those observed in B-FABP–depleted U251 cells, do not appear to be associated with cell migration, as inhibition of these fan-like structures does not affect cell motility [35]. The reduction in cell migration observed on B-FABP depletion is in agreement with B-FABP playing a central role in cell migration.

In vitro ligand-binding studies show that docosahexanoic acid (DHA; 22:*n* − 6) is the preferred ligand of B-FABP [36,37]. DHA is the longest and most highly unsaturated fatty acid found in membranes. Highly unsaturated long-chain fatty acids can alter the structure and function of membranes, increasing their fluidity, elasticity, and permeability, and potentially affecting signal transduction and gene expression [38–40]. Recent data support a role for DHA in the hyperfluidization of membranes [41]. Preferential localization of B-FABP at the leading edges of cells may result in increased DHA content at these sites. Increased fluidity may directly promote

cell motility or may activate cell signaling events associated with cell motility. Future work will involve the characterization of the effect of fatty acid ligands on the growth properties of B-FABP–expressing malignant glioma cells.

B-FABP is primarily located in the nucleus of U251 and B-FABP–transfected U87 cells and can be found in both the cytoplasm and the nucleus of astrocytoma tumor cells, in keeping with a role in the regulation of gene expression. It has been postulated that FABP-bound fatty acids may serve as ligands for peroxisome proliferator–activated receptors (PPARs), which then activate the transcription of genes containing PPAR response elements [42]. PPARs are expressed in malignant glioma cell lines, although their relationship to B-FABP and its fatty acid ligands is not known [43]. A link to PPARs would suggest a direct role for B-FABP and/or its ligands in the regulation of genes involved in cell migration.

In addition to the nucleus, B-FABP localizes to structures associated with actin cytoskeleton remodeling and cell migration, such as stress fibers and sites of focal adhesions (e.g., leading edges) [44]. Proteins involved in cell migration include cadherins, integrins, actin and actin-binding proteins, the Rho family of small GTPases, growth factors, and receptors [45]. Two proteins recently implicated in malignant glioma cell migration include tyrosine kinase Pyk2, which is believed to mediate G protein–coupled receptor activation, and the 8-kDa polypeptide P311, which is proposed to regulate malignant glioma cell motility through the reorganization of the actin cytoskeleton [46,47]. To identify pathways altered as a consequence of B-FABP expression, we compared genes expressed in U87 control and B-FABP–transfected cells. A number of differentially expressed transcripts encoding proteins involved in cell migration and adhesion were identified by cDNA microarray analysis, including cadherins, laminin, tensin, and integrin β_4 (our unpublished data). Based on these preliminary results, we postulate that the mechanism underlying B-FABP–enhanced cell migration will likely involve modulation of cell adhesion properties.

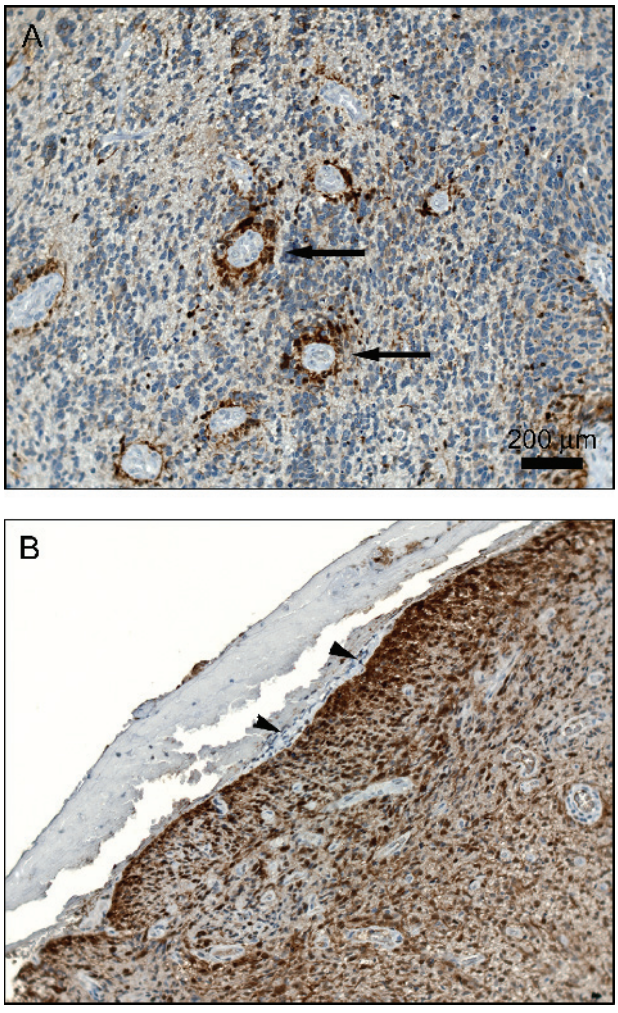

Figure 7. *Immunohistochemical analysis of B-FABP in blood vessels and in the pia surface of grade IV astrocytomas. Tissue sections from patient 1022 (A) and patient 1032 (B) were immunostained with affinity-purified anti–B-FABP antibody and counterstained with hematoxylin. Arrows point to blood vessels surrounded by B-FABP–staining cells. Arrowheads point to the pia mater.*

High-grade astrocytomas are highly invasive within the brain itself; however, metastasis outside the brain is rare. This has been attributed to the short life expectancy of the patient and/or the blood–brain barrier. However, the blood–brain barrier is disrupted in nearly all patients with grade IV astrocytomas [48]. Moreover, the majority of high-grade astrocytoma patients undergo surgery followed by radiation treatment, which are both risk factors for metastasis [49]. Astrocytoma tumor cells have been shown to migrate along white matter tracks, to encircle neurons and blood vessels, and to pile up at the subpial surface of the brain [50,51]. The B-FABP–positive cells observed in highly infiltrative regions of grade IV astrocytomas mimic the previously reported migratory behavior of astrocytoma cells, with B-FABP–positive cells encircling blood vessels and accumulating near the pia mater. Of note, these features (i.e., high motility, association with blood vessels, and white matter tracts) are also properties of neural stem cells and progenitor cells [52].

Migrating B-FABP–positive tumor cells may not be particularly tumorigenic, as suggested by the decreased proliferation rate and reduced anchorage-independent growth of B-FABP–expressing malignant glioma cells. This is consistent with reports indicating that the expression of FABPs, such as intestinal, liver, and adipocyte FABP, is reduced with increasing malignancy, and that FABP expression is generally associated with increased differentiation [53]. The enhanced motility associated with B-FABP–positive tumor cells may thus represent a property associated with the cell of origin of the tumor rather than with a consequence of the malignant process. An intriguing observation is the presence of B-FABP in gemistocytic astrocytes in grade II astrocytomas. Although gemistocytes have a low proliferative index, their presence in low-grade astrocytomas is an indication of poor prognosis, as these tumors rapidly progress to high-grade astrocytomas [22,23]. B-FABP–expressing gemistocytes may, therefore, represent precancerous cells that have the potential to develop into more aggressive cancer cells. Thus, B-FABP–positive gemistocytic astrocytes in low-grade astrocytomas, B-FABP–positive infiltrating tumor cells in high-grade astrocytomas, and B-FABP–

negative proliferating cells in the tumor center may represent transformed glial cells at different stages of the tumorigenic process, each accompanied by progressively more mutations or abnormalities. Loss of B-FABP expression may represent a relatively late tumorigenic event, allowing cells to accumulate at one site due to decreased cell migration.

In conclusion, we have used complementary approaches to demonstrate that B-FABP expression in malignant glioma cells increases migratory activity. Changes in migratory activity are accompanied by morphologic alterations: longer processes in B-FABP–expressing U87 cells and extensive membrane ruffling in the case of B-FABP–depleted U251 cells, suggesting a role for B-FABP in altering membrane properties. Based on transfection experiments and immunohistochemical analyses of astrocytoma tumors, we propose that the spread of astrocytoma cells within the brain is performed through the migration of B-FABP–expressing tumor cells that originate from radial glial cells. Manipulation of B-FABP levels in malignant glioma cells has a dramatic effect on their migratory and growth properties. A better understanding of B-FABP–expressing cells may lead to novel approaches for the treatment of both low-grade and high-grade astrocytomas, perhaps through the manipulation of B-FABP or its ligand DHA. B-FABP may also serve as a useful prognostic marker for astrocytomas, particularly as related to the prediction of tumor spread and recurrence within the brain.

Acknowledgements

We are grateful to Rufus Day III for the U87 and U251 malignant glioma cell lines, and to John Rowe for the affinity purification of the anti–B-FABP antibody. Special thanks to Charlie Hao and Lothar Resch for their help with the pathological analysis of glioblastoma tumors, and to Marcela White and the Brain Tumor Foundation of Canada for grade IV astrocytoma tissue sections.

References

[1] Ohgaki H and Kleihues P (2005). Population-based studies on incidence, survival rates, and genetic alterations in astrocytic and oligodendroglial gliomas. *J Neuropathol Exp Neurol* **6** (64), 479–489.

[2] Pasquier B, Pasquier D, N'Golet A, Panh MH, and Couderc P (1980). Extraneural metastases of astrocytomas and glioblastomas: clinicopathological study of two cases and review of literature. *Cancer* **1** (45), 112–125.

[3] Collignon FP, Holland EC, and Feng S (2004). Organ donors with malignant gliomas: an update. *Am J Transplant* **1** (4), 15–21.

[4] Sanai N, Alvarez-Buylla A, and Berger MS (2005). Neural stem cells and the origin of gliomas. *N Engl J Med* **8** (353), 811–822.

[5] Godbout R, Bisgrove DA, Shkolny D, and Day RS III (1998). Correlation of B-FABP and GFAP expression in malignant glioma. *Oncogene* **15** (16), 1955–1962.

[6] Feng L, Hatten ME, and Heintz N (1994). Brain lipid–binding protein (BLBP): a novel signaling system in the developing mammalian CNS. *Neuron* **4** (12), 895–908.

[7] Kurtz A, Zimmer A, Schnutgen F, Bruning G, Spener F, and Muller T (1994). The expression pattern of a novel gene encoding brain–fatty acid binding protein correlates with neuronal and glial cell development. *Development* **9** (120), 2637–2649.

[8] Schmechel DE and Rakic P (1979). A Golgi study of radial glial cells in developing monkey telencephalon: morphogenesis and transformation into astrocytes. *Anat Embryol (Berl)* **2** (156), 115–152.

[9] Goldman S (2003). Glia as neural progenitor cells. *Trends Neurosci* **11** (26), 590–596.

[10] Glatz JF and Storch J (2001). Unravelling the significance of cellular fatty acid–binding proteins. *Curr Opin Lipidol* **3** (12), 267–274.

[11] Lawrie LC, Dundas SR, Curran S, and Murray GI (2004). Liver fatty acid binding protein expression in colorectal neoplasia. *Br J Cancer* **10** (90), 1955–1960.

[12] Davidson NO, Ifkovits CA, Skarosi SF, Hausman AM, Llor X, Sitrin MD, Montag A, and Brasitus TA (1993). Tissue- and cell-specific patterns of expression of rat liver and intestinal fatty acid binding protein during development and in experimental colonic and small intestinal adenocarcinomas. *Lab Invest* **6** (68), 663–675.

[13] Celis JE, Ostergaard M, Basse B, Celis A, Lauridsen JB, Ratz GP, Andersen I, Hein B, Wolf H, Orntoft TF, et al. (1996). Loss of adipocyte-type fatty acid binding protein and other protein biomarkers is associated with progression of human bladder transitional cell carcinomas. *Cancer Res* **20** (56), 4782–4790.

[14] Adamson J, Morgan EA, Beesley C, Mei Y, Foster CS, Fujii H, Rudland PS, Smith PH, and Ke Y (2003). High-level expression of cutaneous fatty acid–binding protein in prostatic carcinomas and its effect on tumorigenicity. *Oncogene* **18** (22), 2739–2749.

[15] Liang Y, Diehn M, Watson N, Bollen AW, Aldape KD, Nicholas MK, Lamborn KR, Berger MS, Botstein D, Brown PO, et al. (2005). Gene expression profiling reveals molecularly and clinically distinct subtypes of glioblastoma multiforme. *Proc Natl Acad Sci USA* **16** (102), 5814–5819.

[16] Schmid RS, Yokota Y, and Anton ES (2006). Generation and characterization of brain lipid–binding protein promoter-based transgenic mouse models for the study of radial glia. *Glia* **4** (53), 345–351.

[17] Kondraganti S, Mohanam S, Chintala SK, Kin Y, Jasti SL, Nirmala C, Lakka SS, Adachi Y, Kyritsis AP, Ali-Osman F, et al. (2000). Selective suppression of matrix metalloproteinase-9 in human glioblastoma cells by antisense gene transfer impairs glioblastoma cell invasion. *Cancer Res* **24** (60), 6851–6855.

[18] Bigner SH, Bullard DE, Pegram CN, Wikstrand CJ, and Bigner DD (1981). Relationship of *in vitro* morphologic and growth characteristics of established human glioma–derived cell lines to their tumorigenicity in athymic nude mice. *J Neuropathol Exp Neurol* **4** (40), 390–409.

[19] Lauffenburger DA and Horwitz AF (1996). Cell migration: a physically integrated molecular process. *Cell* **3** (84), 359–369.

[20] Fukata M, Nakagawa M, and Kaibuchi K (2003). Roles of Rho-family GTPases in cell polarisation and directional migration. *Curr Opin Cell Biol* **5** (15), 590–597.

[21] Li S, Guan JL, and Chien S (2005). Biochemistry and biomechanics of cell motility. *Annu Rev Biomed Eng* **7**, 105–150.

[22] Watanabe K, Tachibana O, Yonekawa Y, Kleihues P, and Ohgaki H (1997). Role of gemistocytes in astrocytoma progression. *Lab Invest* **2** (76), 277–284.

[23] Yang HJ, Kim JE, Paek SH, Chi JG, Jung HW, and Kim DG (2003). The significance of gemistocytes in astrocytoma. *Acta Neurochir (Wien)* **12** (145), 1097–1103 (discussion, 1103).

[24] Kaloshi G, Mokhtari K, Carpentier C, Taillibert S, Lejeune J, Marie Y, Delattre JY, Godbout R, and Sanson M (2007). FABP7 expression in glioblastomas: relation to prognosis, invasion and EGFR status. *J Neuro-Oncol* **84**, 245–248.

[25] Liang Y, Bollen AW, Aldape KD, and Gupta N (2006). Nuclear FABP7 immunoreactivity is preferentially expressed in infiltrative glioma and is associated with poor prognosis in EGFR-overexpressing glioblastoma. *BMC Cancer* **6**, 97.

[26] Anthony TE, Klein C, Fishell G, and Heintz N (2004). Radial glia serve as neuronal progenitors in all regions of the central nervous system. *Neuron* **6** (41), 881–890.

[27] Hartfuss E, Galli R, Heins N, and Gotz M (2001). Characterization of CNS precursor subtypes and radial glia. *Dev Biol* **1** (229), 15–30.

[28] Merkle FT, Tramontin AD, Garcia-Verdugo JM, and Alvarez-Buylla A (2004). Radial glia give rise to adult neural stem cells in the subventricular zone. *Proc Natl Acad Sci USA* **50** (101), 17528–17532.

[29] Tso CL, Freije WA, Day A, Chen Z, Merriman B, Perlina A, Lee Y, Dia EQ, Yoshimoto K, Mischel PS, et al. (2006). Distinct transcription profiles of primary and secondary glioblastoma subgroups. *Cancer Res* **1** (66), 159–167.

[30] Kriegstein AR (2005). Constructing circuits: neurogenesis and migration in the developing neocortex. *Epilepsia* **46** (Suppl 7), 15–21.

[31] Smith KM, Ohkubo Y, Maragnoli ME, Rasin MR, Schwartz ML, Sestan N, and Vaccarino FM (2006). Midline radial glia translocation and

corpus callosum formation require FGF signaling. *Nat Neurosci* **6** (9), 787–797.
[32] Kakita A (2001). Migration pathways and behavior of glial progenitors in the postnatal forebrain. *Hum Cell* **1** (14), 59–75.
[33] Nadarajah B, Brunstrom JE, Grutzendler J, Wong RO, and Pearlman AL (2001). Two modes of radial migration in early development of the cerebral cortex. *Nat Neurosci* **2** (4), 143–150.
[34] Rinnerthaler G, Geiger B, and Small JV (1988). Contact formation during fibroblast locomotion: involvement of membrane ruffles and microtubules. *J Cell Biol* **3** (106), 747–760.
[35] Heaysman JE, Pegrum SM, and Preston TM (1982). Spreading chick heart fibroblasts. A correlated study using phase contrast microscopy, RIM, TEM and SEM. *Exp Cell Res* **1** (140), 85–93.
[36] Xu LZ, Sanchez R, Sali A, and Heintz N (1996). Ligand specificity of brain lipid–binding protein. *J Biol Chem* **40** (271), 24711–24719.
[37] Balendiran GK, Schnutgen F, Scapin G, Borchers T, Xhong N, Lim K, Godbout R, Spener F, and Sacchettini JC (2000). Crystal structure and thermodynamic analysis of human brain fatty acid–binding protein. *J Biol Chem* **35** (275), 27045–27054.
[38] Stillwell W and Wassall SR (2003). Docosahexaenoic acid: membrane properties of a unique fatty acid. *Chem Phys Lipids* **1** (126), 1–27.
[39] Hashimoto M, Hossain S, Yamasaki H, Yazawa K, and Masumura S (1999). Effects of eicosapentaenoic acid and docosahexaenoic acid on plasma membrane fluidity of aortic endothelial cells. *Lipids* **12** (34), 1297–1304.
[40] Rojas CV, Martinez JI, Flores I, Hoffman DR, and Uauy R (2003). Gene expression analysis in human fetal retinal explants treated with docosahexaenoic acid. *Invest Ophthalmol Vis Sci* **7** (44), 3170–3177.
[41] Valentine RC and Valentine DL (2004). Omega-3 fatty acids in cellular membranes: a unified concept. *Prog Lipid Res* **5** (43), 383–402.
[42] Wolfrum C, Borrmann CM, Borchers T, and Spener F (2001). Fatty acids and hypolipidemic drugs regulate peroxisome proliferator–activated receptors alpha- and gamma-mediated gene expression *via* liver fatty acid binding protein: a signaling path to the nucleus. *Proc Natl Acad Sci USA* **5** (98), 2323–2328.
[43] Kato M, Nagaya T, Fujieda M, Saito K, Yoshida J, and Seo H (2002). Expression of PPARgamma and its ligand-dependent growth inhibition in human brain tumor cell lines. *Jpn J Cancer Res* **6** (93), 660–666.
[44] Maidment SL (1997). The cytoskeleton and brain tumour cell migration. *Anticancer Res* **6B** (17), 4145–4149.
[45] Christofori G (2006). New signals from the invasive front. *Nature* **7092** (441), 444–450.
[46] Lipinski CA, Tran NL, Menashi E, Rohl C, Kloss J, Bay RC, Berens ME, and Loftus JC (2005). The tyrosine kinase pyk2 promotes migration and invasion of glioma cells. *Neoplasia* **5** (7), 435–445.
[47] McDonough WS, Tran NL, and Berens ME (2005). Regulation of glioma cell migration by serine-phosphorylated P311. *Neoplasia* **9** (7), 862–872.
[48] Schneider SW, Ludwig T, Tatenhorst L, Braune S, Oberleithner H, Senner V, and Paulus W (2004). Glioblastoma cells release factors that disrupt blood–brain barrier features. *Acta Neuropathol (Berl)* **3** (107), 272–276.
[49] Hou LC, Veeravagu A, Hsu AR, and Tse VC (2006). Recurrent glioblastoma multiforme: a review of natural history and management options. *Neurosurg Focus* **4** (20), E5.
[50] Holland EC (2000). Glioblastoma multiforme: the terminator. *Proc Natl Acad Sci USA* **12** (97), 6242–6244.
[51] Peiffer J and Kleihues P (1999). Hans-Joachim Scherer (1906–1945), pioneer in glioma research. *Brain Pathol* **2** (9), 241–245.
[52] Holland EC (2001). Progenitor cells and glioma formation. *Curr Opin Neurol* **6** (14), 683–688.
[53] Zimmerman AW and Veerkamp JH (2002). New insights into the structure and function of fatty acid–binding proteins. *Cell Mol Life Sci* **7** (59), 1096–1116.

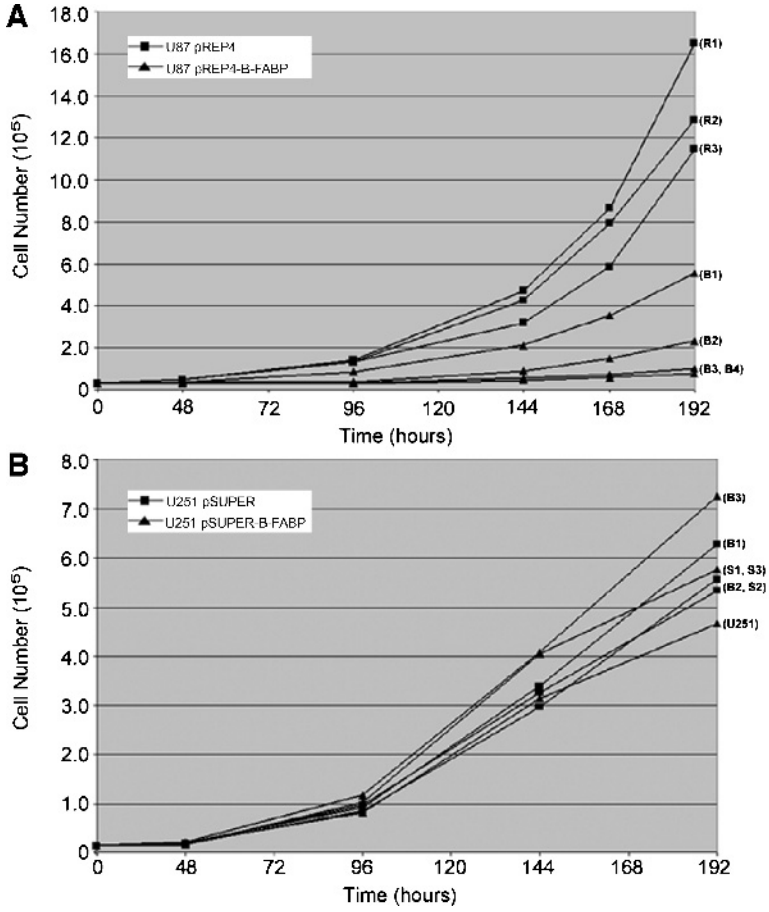

Cell Line	Doubling Time
U87	21.0
pREP4-1	28.0
pREP4-2	32.5
pREP4-3	31.0
pREP4/B-FABP-1	49.0
pREP4/B-FABP-2	49.5
pREP4/B-FABP-3	77.0
pREP4/B-FABP-4	64.5
U251	26.0
pSUPER-1	23.0
pSUPER-2	24.0
pSUPER-3	23.0
pSUPER/B-FABP-1	23.0
pSUPER/B-FABP-2	24.0
pSUPER/B-FABP-3	21.0

Figure W1. *Proliferation of U87- and U251-transfected cells. U87 control and B-FABP–expressing transfectants (A) and U251 control and U251-depleted transfectants (B) were seeded at 15,000 cells/35-mm culture dish. Cells from triplicate plates were counted using a Coulter Particle and Size Analyzer (Beckman Coulter, Fullerton, CA) at 48, 96, 144, 168, and 192 hours after plating. Growth curves were generated using the average of triplicate plates at each time point. Doubling times were obtained using the exponential phase of the growth curves.*

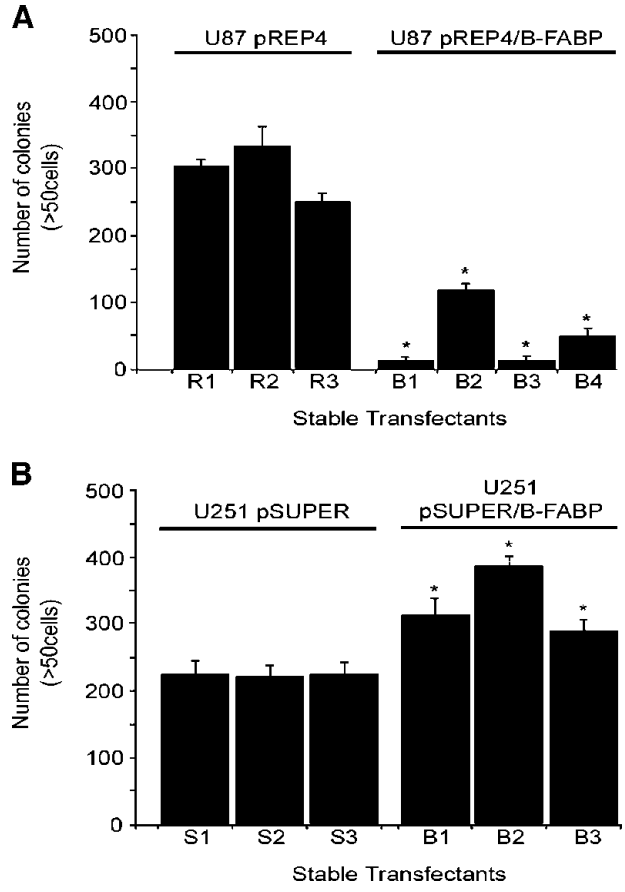

Figure W2. *Growth of U87 and U251 transfectants in soft agar. U87 pREP4 control and pREP4/B-FABP transfectants (A) and U251 pSUPER control and pSUPER/B-FABP transfectants (B) were plated in quadruplicate at 10^3 and 10^4 cells/dish. Colonies (> 50 cells) were counted after 4 weeks of incubation using a Nikon Diaphot 300 light microscope with a 4× objective (Nikon, Tokyo, Japan). Error bars indicate SEM.*